Journal of Inorganic Biochemistry 195 (2019) 61–70

Contents lists available at ScienceDirect

Journal of Inorganic Biochemistry

journal homepage: www.elsevier.com/locate/jinorgbio

Bioinorganic methods

The hydrogen bonding network of coproheme in coproheme decarboxylase from *Listeria monocytogenes*: Effect on structure and catalysis

Lisa Milazzo[a], Thomas Gabler[b], Vera Pfanzagl[b], Hanna Michlits[b], Paul G. Furtmüller[b], Christian Obinger[b], Stefan Hofbauer[b], Giulietta Smulevich[a,*]

[a] Dipartimento di Chimica "Ugo Schiff", Università di Firenze, Via della Lastruccia 3-13, 50019 Sesto Fiorentino, (Fi), Italy
[b] Department of Chemistry, Division of Biochemistry, BOKU – University of Natural Resources and Life Sciences, Muthgasse 18, A-1190 Vienna, Austria

ARTICLE INFO

Keywords:
Coproheme decarboxylase
Heme *b* biosynthesis
Resonance Raman spectroscopy
Propionyl hydrogen-bond
Carbon monoxide

ABSTRACT

Coproheme decarboxylase (ChdC) catalyzes the oxidative decarboxylation of coproheme to heme *b*, i.e. the last step in the recently described coproporphyrin-dependent pathway. Coproheme decarboxylation from *Listeria monocytogenes* is a robust enzymatic reaction of low catalytic efficiency. Coproheme acts as both substrate and redox cofactor activated by H_2O_2. It fully depends on the catalytic Y147 close to the propionyl group at position 2. In the present study we have investigated the effect of disruption of the comprehensive and conserved hydrogen bonding network between the four propionates and heme cavity residues on (i) the conformational stability of the heme cavity, (ii) the electronic configuration of the ferric redox cofactor/substrate, (iii) the binding of carbon monoxide and, (iv) the decarboxylation reaction mediated by addition of H_2O_2. Nine single, double and triple mutants of ChdC from *Listeria monocytogenes* were produced in *E. coli*. The respective coproheme- and heme *b*-complexed proteins were studied by UV–Vis, resonance Raman, circular dichroism spectroscopy, and mass spectrometry. Interactions of propionates 2 and 4 with residues in the hydrophobic cavity are crucial for maintenance of the heme cavity architecture, for the mobile distal glutamine to interact with carbon monoxide, and to keep the heme cavity in a closed conformation during turnover. By contrast, the impact of substitution of residues interacting with solvent exposed propionates 6 and 7 was negligible. Except for Y147A and K151A all mutant ChdCs exhibited a wild-type-like catalytic activity. The findings are discussed with respect to the structure-function relationships of ChdCs.

1. Introduction

Three prokaryotic heme *b* biosynthesis pathways have been described so far: (i) the protoporphyrin-dependent (PPD) pathway, the (ii) coproporphyrin-dependent (CPD) pathway and (iii) the alternative heme biosynthesis (Ahb) pathway [1,2]. Coproheme decarboxylase (ChdC) is an enzyme unique for the most recently described CPD pathway [3], which is mainly utilized by Gram-positive bacteria. It catalyzes the last step of the CPD pathway [1] and decarboxylates two propionate groups at positions 2 (p2) and 4 (p4) of coproporphyrin III (coproheme) to vinyl groups, thereby releasing two carbon dioxide molecules and heme *b*. Interestingly, in ChdC, coproheme is both the substrate and redox cofactor. The reaction is triggered by hydrogen peroxide and can be monitored spectrophotometrically and by mass spectrometry [3–6]. A two-fold excess of hydrogen peroxide in coproheme decarboxylase from *Listeria monocytogenes* (LmChdC) is needed to fully convert coproheme to heme *b* [4], whereas an eight-fold excess is necessary for ChdC from *Staphylococcus aureus* (SaChdC) [6].

Fig. 1 depicts the active site of ChdC with histidine as proximal ligand of coproheme and a conserved mobile glutamine in the distal cavity. We used the structure of GsChdC with Mn-coproheme (pdb-code: 5T2K), instead of that of LmChdC with Fe-coproheme since, as stated previously, the former represents the more appropriate interpretation of the structural data of coproheme decarboxylase [7].

The postulated reaction mechanism involves a catalytic tyrosyl radical in close proximity to p2 formed by oxidation of a postulated Compound I [i.e. oxoiron(IV) porphyryl radical]. Formation of the tyrosyl radical is essential for decarboxylation of both p2 and p4 [8]. A lysine residue, which is H-bonded to p4 was also shown to be important (but not essential) for the catalytic reaction [9] (Fig. 1). Two reaction mechanisms have been postulated: (i) one involves a long range electron transfer for the second decarboxylation at p4 to span the distance from this propionyl group to the catalytic tyrosine; (ii) the second proposed mechanism involves rearrangement (i.e. twist) of the three-

* Corresponding author.
E-mail address: giulietta.smulevich@unifi.it (G. Smulevich).

https://doi.org/10.1016/j.jinorgbio.2019.03.009
Received 28 January 2019; Received in revised form 28 February 2019; Accepted 10 March 2019
Available online 21 March 2019

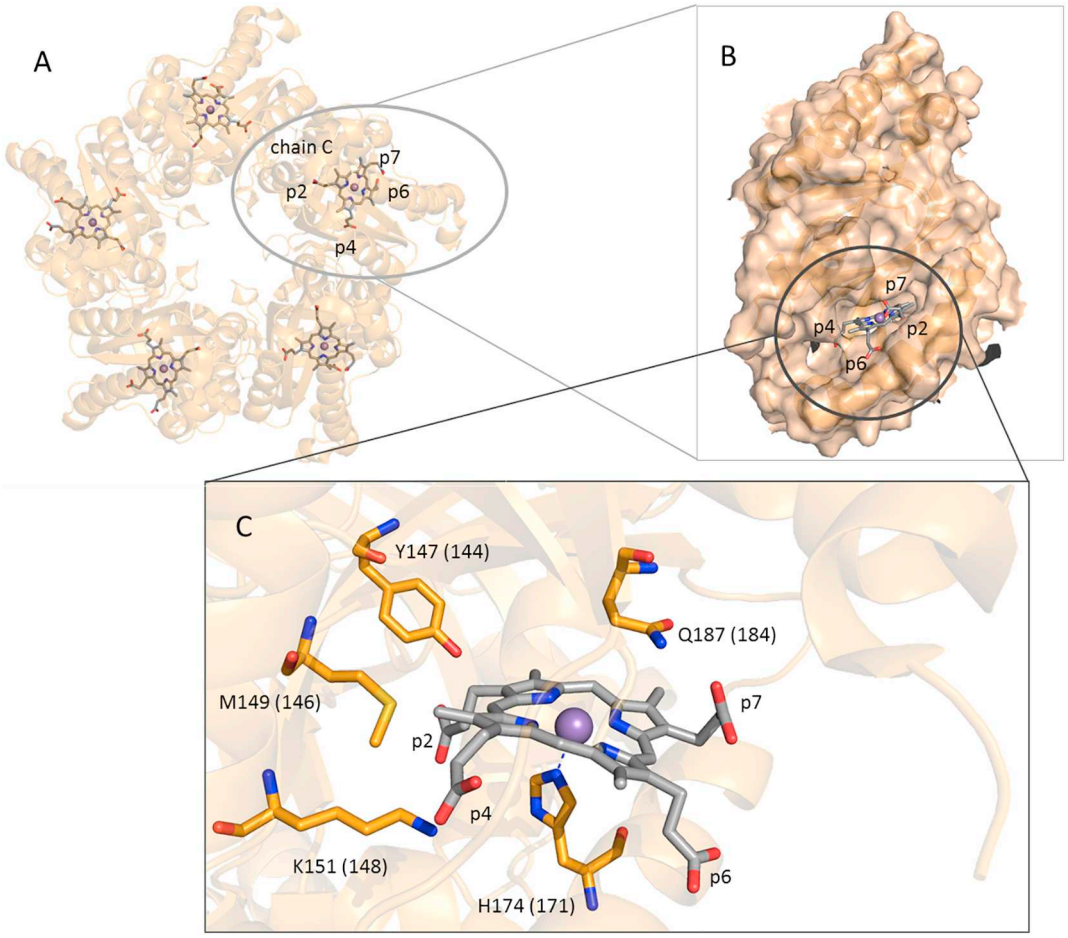

Fig. 1. Structure of coproheme decarboxylase (ChdC). (A) Overall structure of coproheme decarboxylase from *Geobacillus stearothermophilus* (GsChdC) in complex with Mn-coproporphyrin III (pdb-code 5T2K) [9]. (B) Representation of chain C of GsChdC showing solvent exposed propionates p6 and p7. (C) Presentation of the active site of GsChdC with residue numbering for coproheme decarboxylase from *Listeria monocytogenes* (LmChdC) (GsChdC numbering is given in brackets). Fully conserved residues include the catalytic tyrosine 147, methionine 149, lysine 151, mobile distal glutamine 187 and the proximal histidine 174.

propionate intermediate (i.e. monovinyl, monopropionyl deuteroheme) in order for p4 to be positioned in close proximity to the catalytic tyrosine. Experimental data that clearly support either mechanism are still lacking. A twist of the substrate/redox cofactor within the active site would require disruption and re-formation of H-bonding interactions between p4, propionates 6 (p6) and 7 (p7) and the protein moiety. This motivated us to extensively study the H-bonding network of coproheme in LmChdC in its resting state in order to understand its impact on catalysis.

Recently, we have shown that the native ferric form of coproheme decarboxylase from *Listeria monocytogenes* (*Lm*ChdC) is a pentacoordinate quantum mechanically mixed-spin state (5cQS) which is very unusual in biological systems [7]. However, mutation of the Met149 residue to Ala dramatically alters the heme coordination, which becomes a hexacoordinate low-spin (6cLS) species with the amide nitrogen atom of flexible Q187 bound to the heme iron (Fig. 1). Interestingly, the heme *b* product formed upon reaction of the M149A mutant with H_2O_2 consists of two 6cLS species with different resonance Raman (RR) bands [7]. One form (RR ν_3 and ν_2 bands at 1507 and 1588 cm^{-1}, respectively), absent in the Q187A single (Q187A) and double (M149A/Q187A) mutants, is due to the coordination with Q187 at the sixth position. Therefore, it corresponds to the species observed in the coproheme complex of the M149A mutant. The other form (ν_3 and ν_2 bands at 1503 and 1580 cm^{-1}, respectively), is present also in the wild-type protein and the Q187A mutants, has an internal sixth ligand that has not been yet identified. Moreover, upon carbon monoxide binding, the M149A variant showed two CO conformers corresponding to an open (A_0) and a closed (A_1) conformation. The open conformation has been observed in Q187A single and double mutants, while the closed conformation was observed in the wild-type protein. Therefore, we concluded that in the A_1 conformation Q187 is H-bonded to bound carbon monoxide, as previously observed in SaChdC [9]. Interestingly, the open form (A_0) has also been observed in all CO adducts of the heme *b* products (containing two vinyl substituents in positions 2 and 4) of *Lm*ChdC [7]. These data indicate that in the coproheme complex, the interaction between the M149 residue and the propionate in position 2 has an important role in keeping glutamine 187 correctly positioned for the closure of the distal cavity and for the radicalic decarboxylation mediated by Y147.

In the present work we have extended our research to the study of residues involved in the H-bond interactions with the propionate groups in positions 2, 4, 6 and 7 of coproheme in order to understand if other residues, besides M149, are important for the architecture of the catalytic cavity and for catalysis. We found that the interactions between heme cavity residues and propionyls in positions 2 and 4 are crucial to maintain the conformational stability of the active site architecture and to keep the distal glutamine correctly positioned to close the heme cavity. However, they are not essential for the decarboxylation reaction of p2 and p4 per se.

2. Experimental procedures

2.1. Generation of LmChdC variants

Site-directed mutagenesis to obtain LmChdC M149A, Q187A and M149A/Q187A variants using the QuikChange Lightning Kit (Agilent Technologies) was described previously [7]. Generation of LmChdC Y147A, R133A, R179A, K151A, Y113A and Y113A/K151A, Y147A/R220A/S225A variants were produced following the same protocol with the primers listed in Table S1.

2.2. Expression and purification of wild-type LmChdC and variants

LmChdC wild-type and all variants were subcloned into a modified version of the pET21(+) expression vector with an N-terminal StrepII-tag, cleavable by TEV protease, or into a pETM11 expression vector with an N-terminal, TEV cleavable 6 × His-tag, expressed in *E. coli* Tuner (DE3) cells (Merck/Novagen) and purified via a StrepTrap HP or a HisTrap HP 5 mL column (GE Healthcare), as described in detail previously [4].

2.3. Sample preparation for UV–Vis and RR

Ferric coproheme was purchased from Frontier Scientific, Inc. (Logan, Utah, USA) as lyophilized powder. A coproheme solution at pH 7.0 in 50 mM Hepes buffer was prepared by dissolving the coproheme powder in a 0.5 M NaOH solution (ε_{390} = 128,800 M^{-1} cm^{-1}) [10] and then diluting a small aliquot of this concentrated alkaline solution with an appropriate volume of 50 mM Hepes buffer, pH 7.0.

All protein-coproheme complexes were prepared by adding the coproheme solution at pH 7.0 to the apo-proteins dissolved in 50 mM Hepes buffer, pH 7.0. The ferric heme *b*-LmChdC complexes were prepared by adding small aliquots (3–10 μL) of a concentrated solution of H_2O_2 in 50 mM Hepes buffer, pH 7.0 to the corresponding coproheme-LmChdC complex.

The Fe(II)-CO adducts at pH 7.0 were prepared by flushing the ferric coproheme/heme *b* complexes with ^{12}CO (Rivoira, Milan, Italy), and then reducing the coproheme/heme *b* by addition of a freshly prepared sodium dithionite solution (20 mg mL^{-1}).

Sample concentrations, in the range of 40–100 μM for UV–vis and RR measurements, were determined using an extinction coefficient (ε) of 68,000 M^{-1} cm^{-1} at 395 nm (coproheme-WT and mutants) and 76,600 M^{-1} cm^{-1} at 410 nm (heme *b*-LmChdC WT and mutants) [10].

2.4. Electronic absorption

Electronic absorption spectra were recorded using a 5 mm NMR tube (300 nm min^{-1} scan rate) or a 1 mm cuvette (600 nm min^{-1} scan rate) at 25 °C by means of a Cary 60 spectrophotometer (Agilent Technologies) with a resolution of 1.5 nm. For the differentiation process, the Savitzky–Golay method was applied using 15 data points (LabCalc, Galactic Industries, Salem, NH). No changes in the wavelength or in the bandwidth were observed when the number of points was increased or decreased.

2.5. Resonance Raman (RR)

The resonance Raman (RR) spectra were obtained at 25 °C using a 5 mm NMR tube by excitation with the 406.7 and 413.1 nm lines of a Kr^+ laser (Coherent, Innova300 C, Coherent, Santa Clara, CA, USA). Backscattered light from a slowly rotating NMR tube was collected and focused into a triple spectrometer (consisting of two Acton Research SpectraPro 2300i instruments and a SpectraPro 2500i instrument in the final stage with gratings of 3600 grooves/mm and 1800 grooves/mm) working in the subtractive mode, equipped with a liquid nitrogen-cooled CCD detector.

A spectral resolution of 1.2 cm^{-1} and spectral dispersion of 0.40 cm^{-1}/pixel were calculated theoretically on the basis of the optical properties of the spectrometer for the 3600 grating. The RR spectra were calibrated with indene and carbon tetrachloride as standards to an accuracy of 1 cm^{-1} for intense isolated bands. All RR measurements were repeated several times under the same conditions to ensure reproducibility. To improve the signal-to-noise ratio, a number of spectra were accumulated and summed only if no spectral differences were noted. Absorption spectra were measured both prior and after RR measurements to ensure that no degradation occurred under the experimental conditions used. All spectra were baseline-corrected.

2.6. Coproheme decarboxylase activity

In order to test coproheme decarboxylase activity of the LmChdC wild-type (WT) and variants, titrations were performed where small (sub-equimolar) aliquots of H_2O_2 were added to coproheme-ChdCs. In a typical experiment, H_2O_2 was added in 1 μM aliquots to 5 μM coproheme bound to an excess 20 μM ChdC. To ensure complete reaction of the H_2O_2, an interval of at least 15 min was set between each peroxide addition. The titrations were performed in a stirred 1 mL cuvette at room temperature and monitored by UV–vis absorption spectroscopy between 250 and 700 nm, using a scanning photometer (Cary60). The formation of heme *b* was followed by the increase of absorbance at 410 nm and the consumption of coproheme by the decrease of the absorption signal at 395 nm. Mass spectrometric samples were analysed according to previously published protocols [4].

2.7. Secondary structure analysis of wild-type LmChdC and variants

Circular dichroism (CD) spectra of wild-type LmChdC and variants in their apo- and coproheme bound states were recorded (Chirascan, Applied Photophysics, Leatherhead, UK) in the far UV-region (190–260 nm) for secondary structure determination at pH 7.0 (5 mM HEPES buffer, pH 7.0). Conditions were as follows. Spectral bandwidth: 1 nm; scan speed: 10 s nm^{-1}; pathlength: 1 mm; temperature: 20 °C. In order to ensure complete loading of coproheme, enzymes were reconstituted with a slight excess of coproheme and then purified using a size exclusion chromatography step (HiLoad 16/60 Superdex 200 prep grade column, GE Healthcare). The calculation of the ratio of ellipticities at 208 and 222 nm represents the amount of the α-helical secondary structural elements. A lower 208/222 nm ratio represents a higher α-helical content. An increase in the ratio indicates structural rearrangements upon coproheme binding thereby increasing the random coil content [11].

3. Results and Discussion

3.1. The H-bonding network of the coproheme complex of wild-type LmChdC

The active site of LmChdC is defined by several residues that are in hydrogen bonding distance to the four propionates of coproheme. Fig. 2 shows the H-bonding interactions of the propionyl groups in Chain C of the (catalytically inactive) Mn-coproheme structure of ChdC from *Geobacillus stearothermophilus* (GsChdC, 5T2K) [9], which is highly homologous to other Firmicutes (Clade 1) ChdCs including LmChdC. The heme cavity structure reveals an extensive H-bonding network involving p2, p4, p6 and p7, with p6 and p7 being solvent exposed. The H-bonding network is highly conserved throughout Firmicutes ChdCs [2] and also present in LmChdC, which is the target of this study (hydrogen bonding residues in LmChdC: R133, Y147, K151, W159, R179, Q187, R220, S225).

In particular, the propionates 2 and 4, which are decarboxylated to vinyl groups during catalysis, are involved in an extended H-bonding network spanning from p2 to p4 [R220 - water - p2 - S225 - p2 - water -

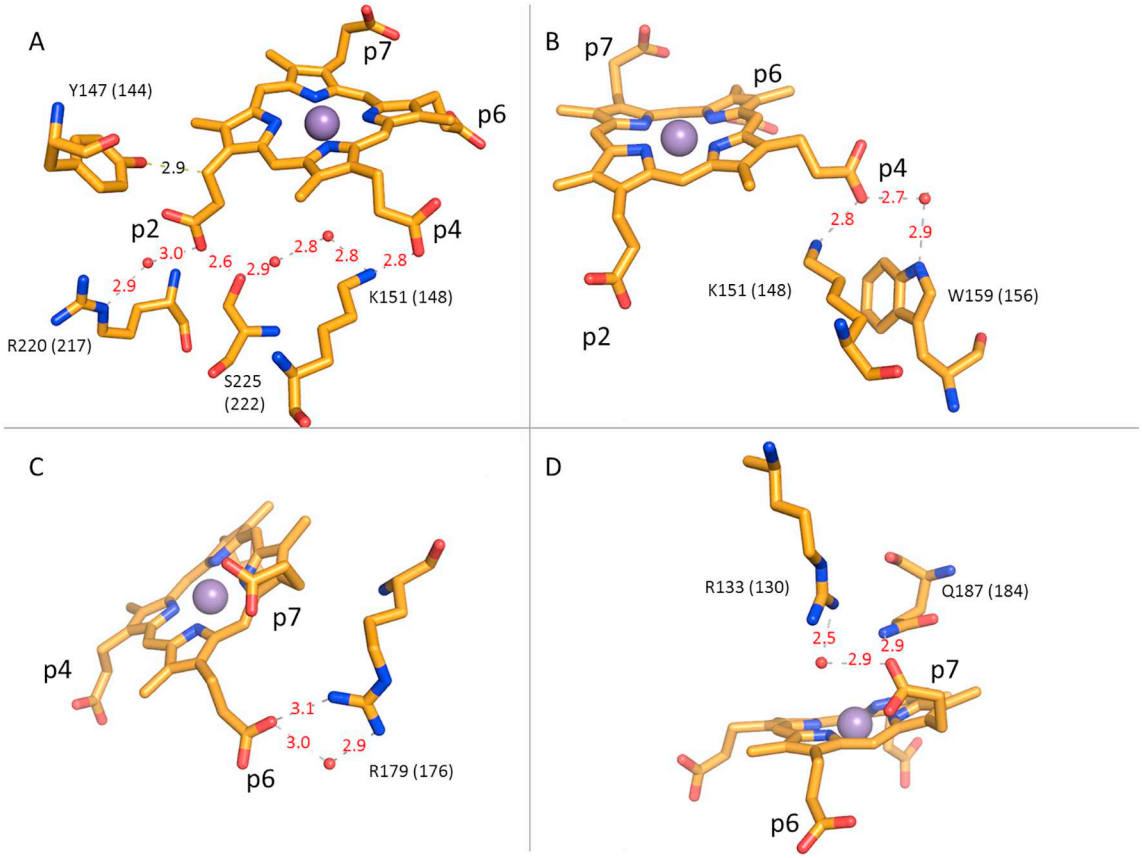

Fig. 2. Hydrogen-bonding network involving the four coproheme propionate groups of Mn-coproheme-GsChdC (chain C, 5T2K) [9]. (A) Propionates at positions 2 (p2) and 4 (p4); (B) p4; (C) solvent exposed propionate at position 6 (p6); and (D) solvent exposed propionate at position 7 (p7). LmChdC numbering is given (GsChdC numbering is given in parentheses).

water - K151 - p4 (GsChdC numbering is given in brackets in Fig. 2)]. Additionally, propionate at position 4 interacts via water-mediated hydrogen-bonds with W159. Furthermore, p4 should be H-bonded via a water with Y113, as is evident from the LmChdC structure (5LOQ), where iron coproheme was refined in a different orientation [4]. In the Mn-coproheme structure of GsChdC (5T2K) this stretch of the sequence is not resolved, since it is part of the flexible loop forming the active site substrate channel [2,12]. The propionate at position 6 (p6) is stabilized by H-bonding mainly to R179, whereas p7 forms an H-bond to Q187 and to R133 via water molecules.

Based on this structural information derived from X-ray crystallography (Fig. 2) we designed and produced several coproheme-LmChdC mutants, besides M149A, which was already shown to exhibit an altered coproheme coordination compared to wild-type LmChdC [7]. In detail, nine single, double and triple mutants were expressed, purified from *E. coli*, and biochemically characterized.

3.2. Disrupting the H-bonding network of coproheme LmChdC – Impact on electronic and overall structure

At first the nine mutants (Y113A, R133A, M149A, K151A, R179A, Q187A, Y113A/K151A, M149A/Q187A, Y147A/R220A/S225A) were analysed spectroscopically. Fig. 3 compares the UV–Vis spectra, the corresponding second derivatives in the Soret region, and the resonance Raman (RR) spectra in the high frequency region of the coproheme-LmChdC mutants with the wild-type protein.

Substitution of the LmChdC residues that interact with the solvent-exposed propionates in positions 6 (R179) and 7 (i.e. Q187 and R133) by alanine does not markedly alter the spin and coordination state of the coproheme iron, as demonstrated by their wild-type-like UV–Vis and RR spectra (Fig. 3, bottom spectra). In fact, upon mutation of Q187 (Q187A and M149A/Q187A) a 6cHS species grows at the expense of the 5cQS species that is predominant in WT, suggesting that a water molecule enters the heme cavity and binds coproheme iron, as indicated by the bands at 1482 (ν_3) and 1614 (ν_{10}) cm^{-1} in the RR spectra and the increase in intensity of the Soret band at 393 nm (396 nm in the D^2 spectrum) of both the Q187A and M149A/Q187A mutants.

Conversely, mutation of the residues interacting with the propionates in position 2 (i.e. Y147, M149, R220 and S225) or position 4 (Y113 and K151, the latter interacts also with p2) alter the heme cavity structure and promote the formation of a 6cLS species. The double (Y113A/K151A) and triple (Y147A/R220A/S225A) mutants (Fig. 3, top spectra) are pure 6cLS hemes. A 6cLS species has been previously observed for the coproheme-M149A complex. Based on this previous finding [7] we propose that the sixth ligand of Y113A/K151A and Y147A/R229A/S225A) might be the amide nitrogen atom of glutamine 187.

Since the disruption of the hydrogen-bonding network of p2 and p4 significantly changed the electronic configuration of the coproheme iron, we further tested the impact of substitution of the amino acids on the overall secondary structure of all the mutant proteins by circular dichroism (CD) measurements in the far UV region. Coproheme binding has a significant impact on protein folding. Comparison of apo- and coproheme-loaded wild-type LmChdC reveals that binding of the substrate (which acts as redox cofactor) increases the overall α-helical content (apo: ~30%; holo: ~33%, calculated using the CDNN software by Applied Photophysics), reflected by a decrease of the ratio of ellipticities at 208 nm and 222 nm (Fig. 4, Fig. S1). Far-UV ECD spectra of apo- and coproheme-LmChdC reported previously showed the same behaviour [10]. Substitution of R133 and Q187 (which interact with p6

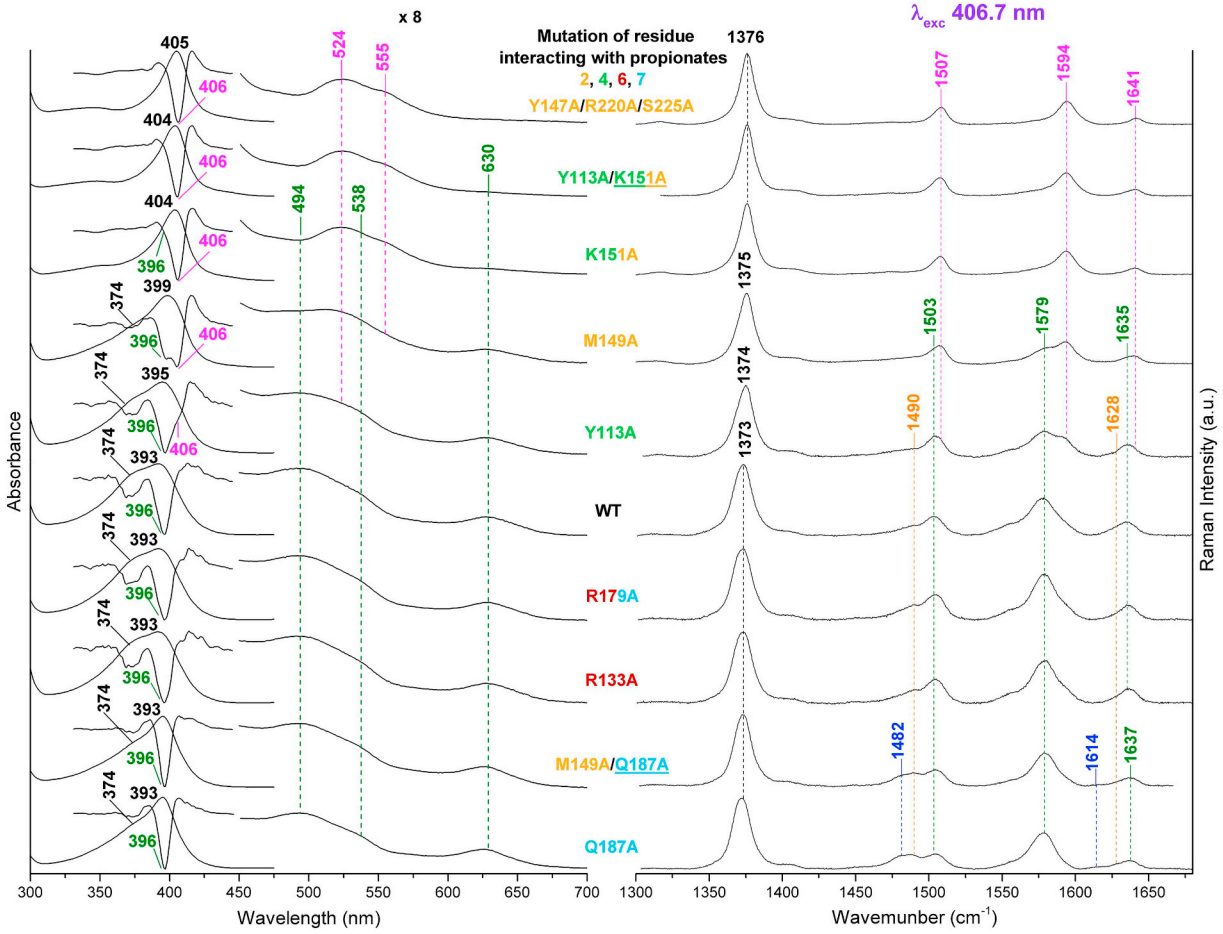

Fig. 3. UV–Vis and resonance Raman characterization of wild-type LmChdC and mutants in complex with coproheme. (Left) UV–Vis and second derivative Soret band spectra (D^2); (right) high frequency region RR spectra (λ_{exc} 406.7 nm). The wavelengths and wavenumbers of the **5cHS**, **5cQS**, **6cHS** and **6cLS** species are highlighted in orange, green, blue and magenta, respectively. The colour of the mutated amino acids (beige, green, brown and light blue) reflect their interaction with propionates at positions **2**, **4**, **6**, and **7**, respectively. The spectra have been shifted along the ordinate axis to allow better visualization. The 450–700 nm region of the UV–Vis spectra is expanded 8-fold. RR experimental conditions: laser power at the sample 5 mW; total accumulation time for each spectrum was 40–140 min.

and p7), Y113 (which forms a water-mediated H-bond to p4 and is located on the flexible loop), as well as the catalytic Y147 (which does not form a H-bond with a propionate, Fig. 2) by alanine has no impact on the spectral changes observed when the apo-proteins are loaded with coproheme. In fact, the mutants R133A, R179A, Q187A and Y113A exhibited a wild-type-like behaviour upon coproheme binding.

By contrast, disruption of the H-bond interactions with p2 and p4 (Y147A/R220A/S225A and K151A) impaired the structural rearrangement when coproheme binds to the respective apo-proteins. The behaviour of the mutant M149A is in between, again emphasizing its importance for maintenance of the active site architecture, despite the fact that it does not form H-bonds with propionates.

When the apo-forms are compared, it becomes evident that catalytic Y147 has an important role in the maintenance of the overall structure of the coproheme-loaded form. Apo-Y147A exhibits a higher content of random coils, and the biggest structural rearrangement upon coproheme binding (Fig. 4, Fig. S1).

3.3. Impact on carbon monoxide binding to ferrous wild-type and mutant proteins

To gain further insight into the impact of disruption of the described H-bonding network we investigated carbon monoxide binding to the respective ferrous mutant proteins. We have previously shown that CO

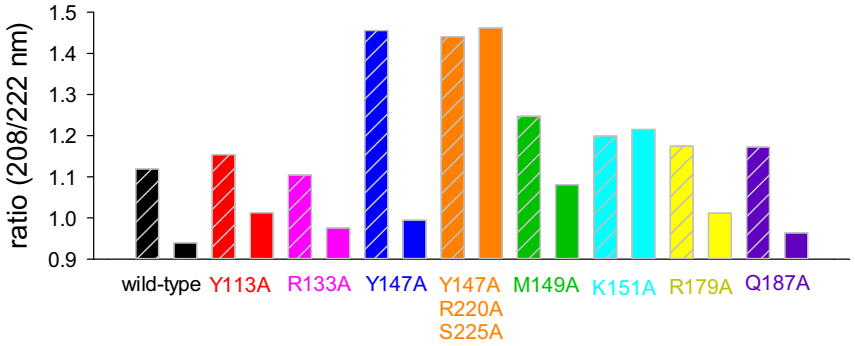

Fig. 4. Structural rearrangement upon coproheme binding to apo-forms of wild-type LmChdC and mutants followed by circular dichroism spectroscopy. Ratios of ellipticities at 208 nm and 222 nm are CD measurements in the far-UV region. Wild-type LmChdC (black) and variants Y113A (red), R133A (magenta), Y147A (blue), Y147A/R220A/S225A (orange), M149A (green), K151A (cyan), R179A (yellow), and Q187A (purple) are presented. Data from apo-proteins are represented by striped bars, data from coproheme bound proteins are represented by bars without stripes.

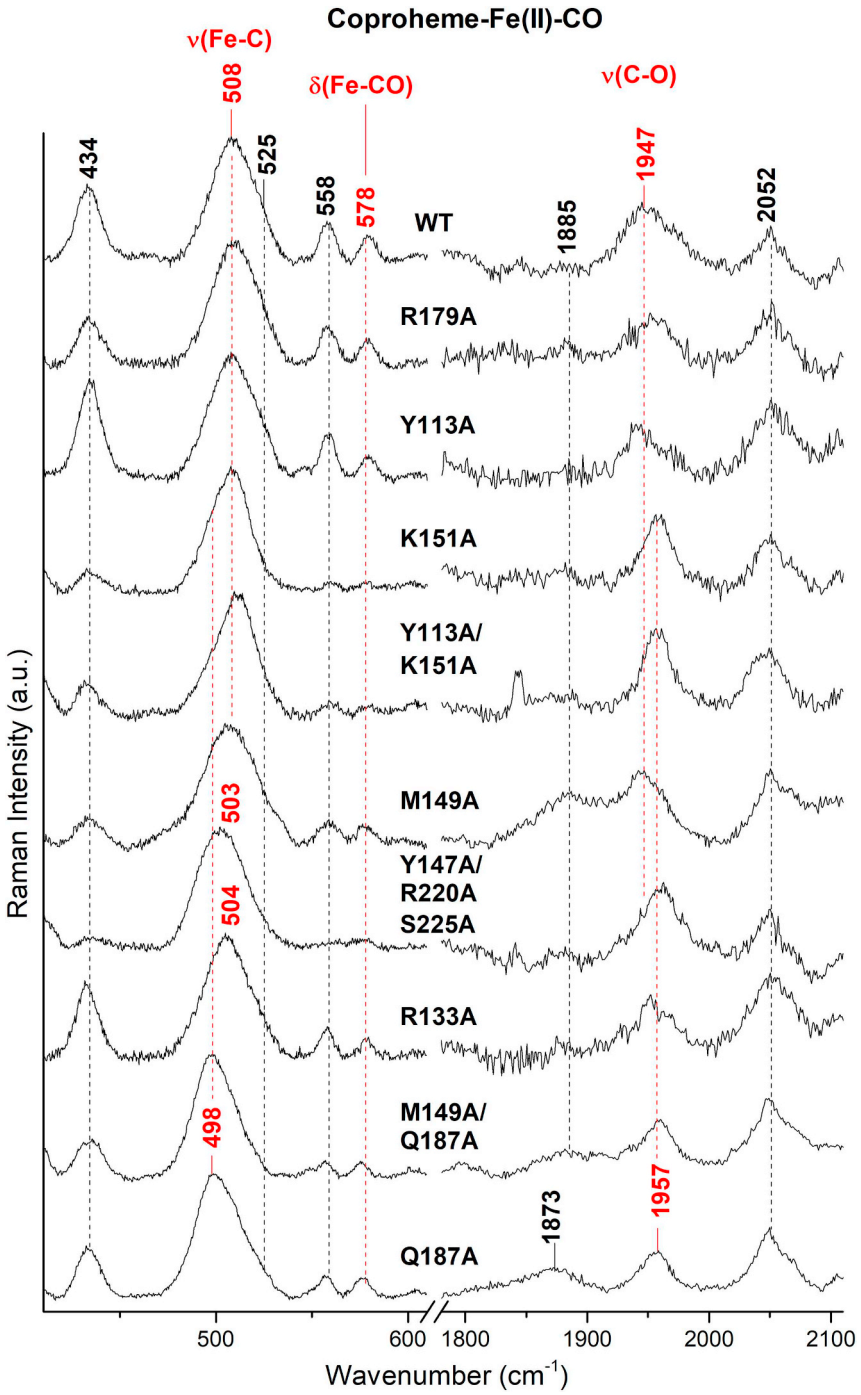

Fig. 5. Resonance Raman (RR) spectra in the low (left) and high (right) frequency regions of the ^{12}CO adducts of the coproheme complexes of wild-type LmChdC and the mutants Q187A, M149A/Q187A, R133A, Y147A/R220A/S225A, M149A, Y113A/K151A, K151A, Y113A and K179A. The frequencies of the ν(FeC), δ(FeCO) and ν(CO) modes are indicated in red. The spectra have been shifted along the ordinate axis to allow better visualization. Experimental conditions: λ_{exc} 413.1 nm, laser power at the sample 1–3 mW; total accumulation time for each spectrum was 60–280 min and 80–220 min in the low and high frequency regions, respectively.

binding to wild-type LmChdC gives rise to the formation of a conformer stabilized by a H-bond with Q187 (closed conformation, A_1), while in the M149A variant both open (A_o) and closed conformations were observed. Therefore, we concluded that the interaction between M149 and propionate 2 has an important role in keeping Q187 correctly positioned to close the distal cavity. Accordingly, in the absence of Q187 or in adducts of all heme *b* forms of ChdC (containing vinyls in positions 2 and 4), only the A_0 conformer was found [7].

Fig. 5 depicts the RR spectra of the CO complexes of all investigated mutants compared with the wild-type protein. The data clearly demonstrate that the carbon monoxide complexes of ferrous Y113A and R179A are almost identical to the wild-type protein, showing RR signatures characteristic of a closed conformation.

By contrast, disruption of the H-bonds with p4 only (K151A and Y113A/K151A) slightly destabilizes the active site structure. In the CO complexes of ferrous K151A and Y113A/K151A a weak open form appears, which becomes more pronounced in the M149A, Y147A/R220A/S225A, and R133A mutants (similar to the recently investigated mutants Q187A and Q187A/M149A [7]). This suggests that in those mutants where a strong open form is observed glutamine 187 is not able

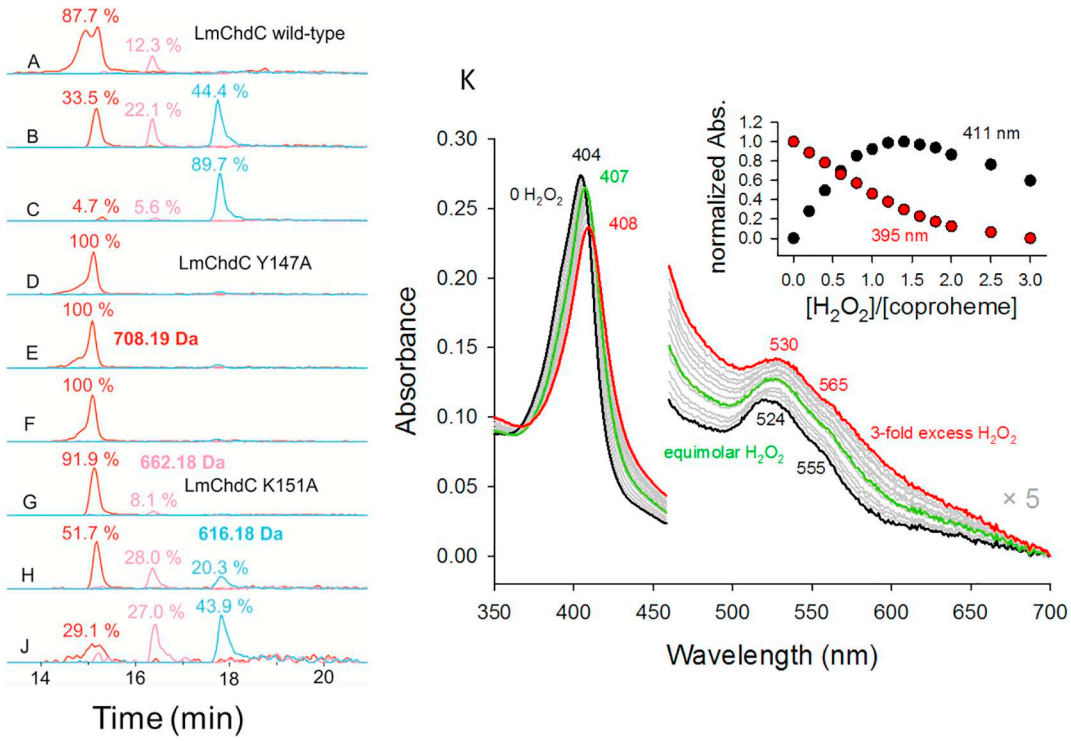

Fig. 6. Catalytic activity of LmChdC variants Y147A and K151A. Mass spectrometric analysis of the activity of wild-type LmChdC in the absence of H_2O_2 (A), at equimolar concentration (B) and 2-fold excess (C) of H_2O_2. AnalogouslyY147A variant is presented in D-F. The same analysis is reported for the LmChdC K151A variant in the absence of H_2O_2 (G), (H) equimolar concentration of H_2O_2, (J) 2-fold excess of H_2O_2. The mass of coproheme (708.19 Da) is indicated in red, of monovinyl, monopropionyl deuteroheme (662.18 Da) in pink, and of heme *b* (616.18 Da) in cyan. (K) Shows the spectral conversion of coproheme to heme *b* of K151A variant mediated by H_2O_2; black, starting spectrum of low-spin coproheme; green, spectrum at equimolar concentration of H_2O_2; red, spectrum after addition of a 3-fold excess of H_2O_2. The inset represents normalized absorbance changes at 395 nm and 411 over the course of the hydrogen peroxide titration.

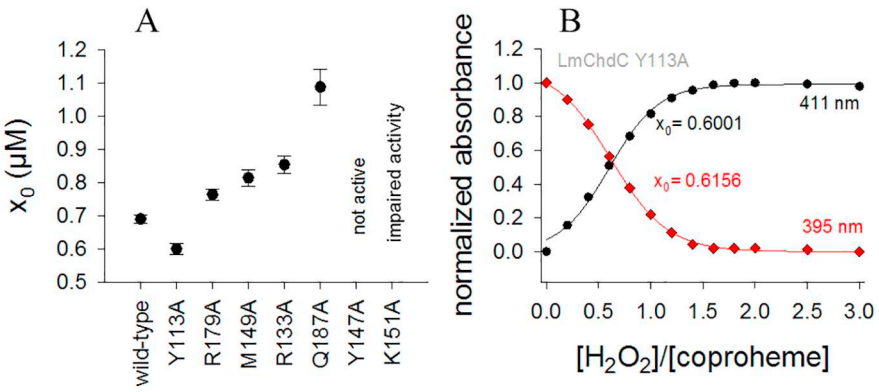

Fig. 7. Hydrogen peroxide-triggered conversion of coproheme to heme *b* mediated by wild-type LmChdC and mutants. (A) Turning points of sigmoidal fits (x_0) at 411 nm. A low value represents efficient catalysis, as less hydrogen peroxide is needed for complete conversion. (B) Plot of normalized absorbances at 395 nm (red, coproheme) and 411 nm (black, heme *b*) with sigmoidal fits versus the ratio $[H_2O_2]/[coproheme]$. The titration of the variant Y113A is presented as a representative example.

to interact strongly with bound carbon monoxide. The effect is strong in the triple mutant (Y147A/R220A/S225A), where the extended H-bond network spanning from p2 to p4 is affected, as well as in R133A. The interaction between R133 and the water molecule, which is in turn H-bonded to p7 (Fig. 2), seems to be important for keeping Q187 (which is also H-bonded to p7) correctly positioned to close the distal cavity.

3.4. Impact on catalytic activity

The catalytic activity of wild-type LmChdC and the nine mutants was measured by mass spectrometry by following the stepwise decarboxylation of coproheme (708.2 kDa) via the three-propionate intermediate (i.e. monovinyl, monopropionyl deuteroheme, 662.2 kDa) to heme *b* (616.2 kDa). With wild-type LmChdC and all variants (except Y147A, Y147A/R220A/R225A and K151A) a ratio of $[H_2O_2]/[coproheme]) \geq 2$ led to almost complete conversion of coproheme to heme *b* (data not shown).

Fig. 6A–C show the conversion of coproheme to heme *b* via the three-propionate intermediate for LmChdC WT, Fig. 6D–F demonstrate that the Y147A mutant is completely inactive, whereas the decarboxylation activity of K151A is highly impaired (Figs. 6G–J) and it cannot be followed as for the other variants and wild-type LmChdC. In the K151A mutant heme bleaching starts at an approximately equimolar H_2O_2/coproheme ratio (inset to Fig. 6K), prior to the complete conversion of coproheme to heme *b*.

Additionally, we have studied the catalytic activity spectroscopically by following the decrease in concentration of coproheme at 395 nm and the concomitant increase in concentration of heme *b* at 411 nm as described recently [9] and shown in Fig. 6K for K151A as an example. As already seen in the mass spectrometric study, the efficiency of conversion of coproheme to heme *b* of all mutants remains *similar* to that of the WT or slightly decreased except for Y147A, Y147A/R220A/

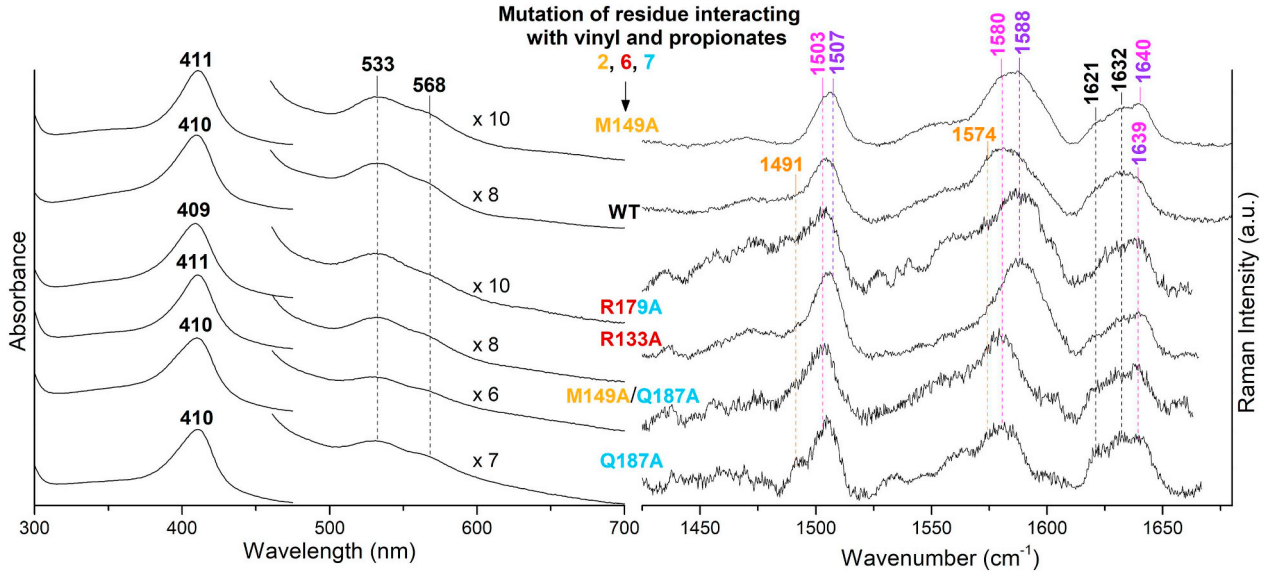

Fig. 8. Comparison of the heme *b*-LmChdC complexes of the wild-type LmChdC and the mutants Q187A, Q187A/M149A, R133A, R179A and M149A. (Left) UV–Vis and (right) high frequency RR spectra (λ_{exc} 413.1 nm). The frequencies of the **5cHS**, and the two **6cLS** species with the N atom of Gln187 and of a sixth ligand not yet identified, are reported in **orange**, **violet** and **magenta**, respectively. The labels of the mutated residues interacting with the vinyl in positions **2**, and the propionates in position **6**, and **7** are reported in beige, brown and light blue, respectively. The 460–700 nm region of the UV–Vis spectra is expanded from 6 to 8-fold as reported for each spectrum. RR experimental conditions: laser power at the sample 5–10 mW, total accumulation time for each spectrum was 100–130 min.

R225A and K151A (Fig. 7). Due to heme bleaching caused by addition of stoichiometric excess of hydrogen peroxide, Michaelis-Menten kinetic parameters are not reliable for comparison [4]. Titrations, starting in the sub-equimolar concentration range (ratio $[H_2O_2]$/[coproheme]), revealed a 2:1 stoichiometry for all variants, except for Q187A, which follows a 3:1 stoichiometry [7]. This is reflected by comparison of x_0 values of the corresponding sigmoidal fits derived from plotting the absorbances at 395 nm (coproheme) and 411 nm (heme *b*) versus the course of titration. The x_0 values are the H_2O_2 to coproheme ratios which represent the inflection point of the sigmoidal fit at which the absorbance change from coproheme to heme *b* is at 50%.

3.5. UV–vis and RR spectra of wild-type and mutant LmChdC complexed with heme b

The hydrogen peroxide-mediated reaction of LmChdC converts the propionate groups in positions 2 and 4 into vinyl groups. Typically, a 6cLS heme *b* is formed. The formation of the vinyl groups upon decarboxylation of coproheme leads to an overall red-shift of the electronic absorption spectra compared to the respective coproheme complexes (Fig. 8, right), and to the appearance of two ν(C=C) vinyl stretching modes in the high frequency region of the RR spectrum at 1621 and 1632 cm^{-1}, together with core size marker bands characteristic of a 6cLS species (1503 (ν_3), 1580 (ν_2), 1639–40 (ν_{10}) cm^{-1}) (Fig. 8, left). A vinyl stretching frequency of 1632 cm^{-1} is quite high and indicates a fairly low degree of conjugation between the vinyl double bond and the porphyrin macrocycle [13]. As a consequence the Soret maxima of wild-type heme *b*-LmChdC and of the respective mutant complexes (409–410 nm) are blue-shifted by about 4–5 nm compared to the myoglobin-imidazole complex, which is a 6cLS species characterized by two conjugated vinyl groups (Soret maximum at 414 nm and both vinyl bands coincident at 1621 cm^{-1}) [14]. The visible bands of wild-type heme *b*-LmChdC and the respective mutant complexes are very similar (533/568 nm) to those of the myoglobin-imidazole complex (535/567 nm) [14], indicating that the sixth ligand is a nitrogen atom. However, the ν_2 region of the RR spectra, allows us to clearly identify two different 6cLS species. In the RR spectra of the wild-type heme *b*-complex and the respective M149A, R133A, and R179A complexes, one species, which is absent in the heme *b*-Q187A and heme *b*-M149A/Q187A complexes, contains Gln187 as distal residue (violet, ν_3 and ν_2 at 1507 and 1588 cm^{-1}, respectively) [7]. The other 6cLS species is present in all complexes but is strongly decreased in R133A, and R179A variants (magenta, ν_3 at 1503 and 1580 cm^{-1}, respectively). The sixth ligand of this species has not been yet identified. The UV–Vis titration between pH 7 and 10 and the RR spectra of the heme *b*-LmHemQ M149A complex (Figs. S2), rule out the possibility that the second LS species derives from a hydroxo-ligated form. In analogy to the coproheme complex [7], heme *b* is released from the cavity at alkaline pH.

4. Conclusions

The present study gives a thorough in-depth picture of the active site of LmChdC in Firmicutes ChdCs, which contains several conserved amino acid residues that interact with the four negatively charged propionates of coproheme (Fig. 2) [2,15] thereby forming salt bridges (p4 - K151, p6 - R179, p7 - R133) and hydrogen bonds (p2 - S225, p2 - water R220, p7 – Q187). Upon decarboxylation of p2 and p4 by ChdC these non-covalent interactions are stepwise disrupted and (partially) re-established, finally leading to heme *b*-ChdC, which has a lower conformational stability compared to coproheme-ChdCs [10] and – due to less non-covalent interactions- easily escapes from the active site.

Decarboxylation is initiated by addition of hydrogen peroxide that mediates the postulated formation of Compound I [oxoiron(IV)coproporphyryl radical]. In wild-type LmChdC Compound I does not accumulate due to conversion into Compound I* [oxoiron(IV) Y147$^{\bullet}$], which attacks p2 and initiates the radicalic decarboxylation reaction. It is important to recall that substitution of Y147 by alanine completely inactivates all the ChdCs studied so far [7,8].

Due to the absence of a base for deprotonation of H—O—O—H at the hydrophobic distal cavity, Compound I formation in ChdC is very slow compared to heme peroxidases or catalases [15–18]. As a consequence, ChdCs are prone to heme bleaching in the presence of excess hydrogen peroxide. Transient stabilization of H_2O_2 (similar to CO binding investigated in the present work) and promotion of the closed conformation (in the CO complex) by Q187 could play an important role in this (most probably) rate-limiting step that initiates the first decarboxylation reaction. Disruption of the H-bonding network involving p2 and p4 seems to impair the role of Q187, as indicated by the

formation of both an open conformation (in the CO complex) and low-spin coproheme, upon mutation, due to Q187 acting as distal ligand of coproheme. Complete disruption of the H-bonding network spanning from p2 to p4 (as in the triple mutant Y147A, R220A and S225A) or elimination of the fully conserved salt bridge between K151 and p4 impairs correct folding of the active site after coproheme uptake by the apo-protein and, finally, significantly diminishes the decarboxylation activity. In addition, M149 and Y147, although not directly involved in the hydrogen bonding network, have been shown to be important for maintenance of the heme cavity architecture [7–9]. Additionally, as outlined above, Y147 is essential for Compound I* formation and, finally, for oxidative attack of p2. Improper coproheme binding due to disruption of the H-bonding network together with impaired Compound I* formation and/or p2 oxidation by $^{\bullet}$Y147 could increase the lifetime of Compound I or Compound I* and thus be responsible for the more pronounced sensitivity to heme bleaching of the mutated proteins compared to wild-type LmChdC.

Disruption of H-bonding partners of solvent-exposed p6 and p7 did not affect the conformational stability or the electronic configuration of coproheme and the catalytic activity of those variants is similar to that of the WT. Additionally, except for R133A, the impact on CO binding was negligible. Substitution of R133 (which interacts with both p7, and, via a bridging water, with Q187) by alanine destabilizes the wild-type-like closed conformation, thus underlining the importance of this mobile distal residue in ligand binding and governing substrate accessibility to the active site.

The catalytic efficiency of coproheme conversion in ChdCs from Firmicutes is generally low (approximately $10^2\,M^{-1}\,s^{-1}$) [4,6]. In the first turnover propionate at position 2 is converted to a vinyl group, thereby disrupting the non-covalent interactions involving R220 and S225 and forming a three-propionate intermediate that can be determined by mass spectrometry ([4], and this paper). Whether this intermediate product stays in place and the second decarboxylation at p4 follows the same mechanism including a long-range electron transfer to $^{\bullet}$Y147 or whether the three-propionate substrate/redox cofactor rearranges (i.e. twists) [and p4 occupies the position of former p2 and comes into optimum distance to $^{\bullet}$Y147] is not clear at the moment. Both reactions need a second H_2O_2 molecule for initiation of the reaction sequence ferric LmChdC → Compound I → Compound I*.

In the second proposed scenario, K151 would change binding partner and interact with p6 instead of p4. It is worth mentioning that this interaction is plausible and evident from inspection of the LmChdC structure (5LOQ) where iron coproheme was refined in a different orientation.

In summary, this study emphasizes that LmChdC has a highly specific coproheme binding pocket, which is sensitive to its surroundings and has significantly altered spectroscopic signatures upon disruption of its H-bonding network. Interactions of p2 and p4 with the protein moiety guarantee the correct and stable resting state of coproheme-bound LmChdC. On the other hand, loss of activity or a significant decrease in catalytic turnover can only be achieved when the radical mechanism is targeted and is not significantly influenced by the spin state of the coproheme iron. In short, disruption of the H-bonding network between LmChdC and coproheme does not impair catalysis. In the case of a rearrangement of the transiently produced three-propionate intermediate during catalysis, in order to bring p4 closer to the catalytic tyrosine, all H-bonds would need to be temporarily disrupted. Coproheme decarboxylation by LmChdC is a robust enzymatic reaction of low catalytic efficiency. This observation implies that this reaction potentially is highly regulated and that the exact organization of the enzymatic machinery for heme biosynthesis in *Listeria monocytogenes* remains unknown. Mechanistic details and other open questions will be the subject of further investigation.

Abbreviations

ChdC coproheme decarboxylase
GsChdC coproheme decarboxylase from *Geobacillus stearothermophilus*
LmChdC coproheme decarboxylase from *Listeria monocytogenes*
SaChdC coproheme decarboxylase from *Staphylococcus aureus*
WT wild-type
LS low-spin
HS high-spin
QS quantum mechanically mixed-spin state
6c six coordinate
5c five coordinate
RR resonance Raman
CD circular dichroism
p2, p4, p6 and p7 propionates at heme positions 2, 4, 6 and 7, respectively

CRediT authorship contribution statement

Lisa Milazzo: Conceptualization, Data curation, Formal analysis, Writing - review & editing, Investigation, Methodology. **Thomas Gabler:** Data curation, Formal analysis. **Vera Pfanzagl:** Formal analysis. **Hanna Michlits:** Data curation. **Paul G. Furtmüller:** Writing - review & editing. **Christian Obinger:** Conceptualization, Writing - review & editing. **Stefan Hofbauer:** Conceptualization, Data curation, Formal analysis, Project administration, Writing - review & editing, Investigation, Methodology, Supervision, Funding acquisition, Writing - original draft. **Giulietta Smulevich:** Conceptualization, Formal analysis, Project administration, Writing - review & editing, Methodology, Supervision, Writing - original draft.

Acknowledgements

This project was supported by the Austrian Science Fund, FWF [Doctoral Program BioToP - Molecular Technology of Proteins (W1224) and the project P29099]. We thank Daniel Maresch for technical support performing mass spectrometry analysis.

Appendix A. Supplementary data

Supplementary data to this article can be found online at https://doi.org/10.1016/j.jinorgbio.2019.03.009.

References

[1] H.A. Dailey, T.A. Dailey, S. Gerdes, D. Jahn, M. Jahn, M.R. O'Brian, M.J. Warren, Microbiol. Mol. Biol. Rev. 81 (2017) (e00048-16).
[2] Pfanzagl, L. Holcik, D. Maresch, G. Gorgone, H. Michlits, P.G. Furtmüller, S. Hofbauer, Arch. Biochem. Biophys. 640 (2018) 27–36.
[3] H.A. Dailey, S. Gerdes, T.A. Dailey, J.S. Burch, J.D. Phillips, Proc. Natl. Acad. Sci. U. S. A. 112 (2015) 2210–2215.
[4] S. Hofbauer, G. Mlynek, L. Milazzo, D. Puhringer, D. Maresch, I. Schaffner, P.G. Furtmuller, G. Smulevich, K. Djinovic-Carugo, C. Obinger, FEBS J. 283 (2016) 4386–4401.
[5] S.A. Lobo, A. Scott, M.A. Videira, D. Winpenny, M. Gardner, M.J. Palmer, S. Schroeder, A.D. Lawrence, T. Parkinson, M.J. Warren, L.M. Saraiva, Mol. Microbiol. 97 (2015) 472–487.
[6] A.I. Celis, B.R. Streit, G.C. Moraski, R. Kant, T.D. Lash, G.S. Lukat-Rodgers, K.R. Rodgers, J.L. DuBois, Biochemistry 54 (2015) 4022–4032.
[7] L. Milazzo, S. Hofbauer, B.D. Howes, T. Gabler, P.G. Furtmüller, C. Obinger, G. Smulevich, Biochemistry 57 (2018) 2044–2057.
[8] B.R. Streit, A.I. Celis, G.C. Moraski, K. Shisler, E.M. Shepard, K.R. Rodgers, G.S. Lukat-Rodgers, J.L. DuBois, J. Biol. Chem. 293 (2018) 3989–3999.
[9] A.I. Celis, G.H. Gauss, B.R. Streit, K. Shisler, G.C. Moraski, K.R. Rodgers, G.S. Lukat-Rodgers, J.W. Peters, J.L. DuBois, J. Am. Chem. Soc. 139 (2017) 1900–1911.
[10] S. Hofbauer, M. Dalla Sega, S. Scheiblbrandner, Z. Jandova, I. Schaffner, G. Mlynek,

K. Djinovic-Carugo, G. Battistuzzi, P.G. Furtmuller, C. Oostenbrink, C. Obinger, Biochemistry 55, (2016) 5398–5412.
[11] S.M. Kelly, T.J. Jess, N.C. Price, Biochim. Biophys. Acta 1751 (2005) 119–139.
[12] S. Hofbauer, A. Hagmüller, I. Schaffner, G. Mlynek, M. Krutzler, G. Stadlmayr, K.F. Pirker, C. Obinger, H. Daims, K. Djinović-Carugo, P.G. Furtmüller, Arch. Biochem. Biophys. 574 (2015) 36–48.
[13] M. Marzocchi, G. Smulevich, J. Raman Spectrosc. 34 (2003) 725–736.
[14] A. Feis, L. Tofani, G. De Sanctis, M. Coletta, G. Smulevich, Biophys. J. 92 (2007) 4078–4087.
[15] M. Zámocký, S. Hofbauer, I. Schaffner, B. Gasselhuber, A. Nicolussi, M. Soudi, K.F. Pirker, P.G. Furtmüller, C. Obinger, Arch. Biochem. Biophys. 574 (2015) 108–119.
[16] C. Obinger, Arch. Biochem. Biophys. 525 (2012) 93–94.
[17] C. Obinger, Arch. Biochem. Biophys. 574 (2015) 1–2.
[18] C. Hawkins, C. Obinger, Arch. Biochem. Biophys. 655 (2018) 55.